

Contents lists available at ScienceDirect

# **BBA** - Biomembranes

journal homepage: http://ees.elsevier.com



# Examination of pH dependency and orientation differences of membrane spanning alpha helices carrying a single or pair of buried histidine residues

Fahmida Afrose, Ashley N. Martfeld <sup>1</sup>, Denise V. Greathouse, Roger E. Koeppe II \*

Department of Chemistry and Biochemistry, University of Arkansas, Fayetteville, AR 72701, USA

#### ARTICLE INFO

## Keywords

Transmembrane helix reorientation Histidine ionization Side chain snorkeling Solid-state deuterium NMR

#### ABSTRACT

We have employed the peptide framework of GWALP23 (acetyl-GGALWLALALALALALALALALAMAGA-amide) to examine the orientation, dynamics and pH dependence of peptides having buried single or pairs of histidine residues. When residues L8 is substituted to yield GWALP23-H8, acetyl-GGALWLAH8ALALALALAL WLAGA-amide, the deuterium NMR spectra of <sup>2</sup>H-labeled core alanine residues reveal a helix that occupies a single transmembrane orientation in DLPC, or in DMPC at low pH, yet shows multiple states at higher pH or in bilayers of DOPC. Moreover, a single histidine at position 8 or 16 in the GWALP23 framework is sensitive to pH. Titration points are observed near pH 3.5 for the deprotonation of H8 in lipid bilayers of DLPC or DMPC, and for H16 in DOPC. When residues L8 and L16 both are substituted to yield GWALP23-H<sup>8,16</sup>, the <sup>2</sup>H NMR spectra show, interestingly, no titration dependence from pH 2-8, yet bilayer thickness-dependent orientation differences. The helix with H8 and H16 is found to adopt a transmembrane orientation in thin bilayers of DLPC, a combination of transmembrane and surface orientations in DMPC, and then a complete transition to a surface bound orientation in the thicker DPoPC and DOPC lipid bilayers. In the surface orientations, alanine A7 no longer fits within the core helix. These results along with previous studies with different locations of histidine residues suggest that lipid hydrophobic thickness is a first determinant and pH a second determinant for the helical orientation, along with possible side-chain snorkeling, when the His residues are incorporated into the hydrophobic region of a lipid membrane-associated helix.

## 1. Introduction

Many important functional roles such as pH sensing, ligand binding and metal transport in the transmembrane domains of membrane proteins may be served by histidine [1–3]. The unique structural characteristics of histidine that combine properties of both polar and aromatic residues as well as its participation in a variety of intermolecular interactions make histidine a highly versatile amino acid [4,5]. Indeed, the histidine side chain engages in several aromatic interactions with neighboring residues which help to stabilize proteins [4,6–8]. The crucial role of His residues for the activation [9] and selectivity [10] of the M2 proton channel of influenza A is well established. The pH dependency of the histidine imidazole side chain is equally important for functions of a variety of membrane proteins. For example, the protonation of some histidine residues in *Diphtheria* toxin triggers conforma-

tional changes of the T domain [11,12] that are necessary for catalysis. The electrostatic repulsion between protonated states of two histidine residues, H257 and H223, initiates the initial conformational change [13]. In case of prion proteins, whose misfolding is believed to be the cause of a group of rare and fatal neurodegenerative diseases [14], the protonation of some important histidine residues destabilizes the proteins [15].

Several related model amphipathic peptide helices with four histidines have been observed to transition from transmembrane to a surface state typically with a midpoint near pH 6 [16–18], with the lipid head group identity and the bilayer thickness also influencing the transition [19]. Other model helices with multiple lysines or even one Arg residue also transition between transmembrane and surface orientations [20–23], as do antimicrobial peptides such as zervamicin [24],

Abbreviations: DLPC, 1,2-dilauroyl-sn-glycero-3-phosphocholine; DMPC, 1,2-dimyristoylphosphatidylcholine; DPOPC, 1,2-dipalmitoleoyl-sn-glycero-3-phosphocholine; DOPC, 1,2-dipalmitoleoyl-sn-glycero-3-phosphocholine; Fmoc, fluorenylmethoxycarbonyl; TFA, trifluoroacetic acid; GALA, geometric analysis of labeled alanines; GWALP23, acetyl-GGALW(LA)6L-WLAGA-[ethanol]amide; RMSD, root mean squared deviation.

 $<sup>\</sup>ensuremath{^{\circ}}$  Corresponding author.

E-mail address: rk2@uark.edu (R.E. Koeppe)

Present Address: CATO SMS, 4364 South Alston Avenue, Durham, NC 27713

F. Afrose et al.

BBA - Biomembranes xxx (xxxxx) xxxx-xxx

alamethecin [24] and PGLa [25], and a channel-forming Leu-Ser peptide [26].

To explore further the influence of individual histidine residues on transmembrane peptide helix behavior, especially when located within the hydrophobic region of membranes, we have utilized the well-studied framework of GWALP23 (acetyl-GGALW[LA]<sub>6</sub>LWLAGA-amide). Many sequence variants of this host helical peptide have been reported and characterized. For example, the presence of more than two interfacial Trp or Tyr residues tends to increase the extent of motional averaging [27,28], while the level of dynamic averaging remains low with only two interfacial tryptophans, at positions 5 and 19, on the same face of the helix [29]. Moreover, the presence of a charged residue, whether lysine[30] or arginine, [21,31] causes dramatic effects when located within the central region of the helix.

The advantages of the GWALP23 framework are not limited to studies of the influence of specific amino acid residues upon the overall behavior of the peptide helix. GWALP23 also has been employed to reveal the pKa values of several membrane-embedded charged residues including histidine [32], glutamic acid [33], lysine [30] and arginine [30,31] in the lipid membrane environment. In several of the studies, a positively charged side chain located close to the center of a transmembrane helix sequence is found to titrate with a pKa value that is about 2-4 pH units lower than the standard value in aqueous solution [30,32]. Nevertheless, the arginine side chain is observed not to titrate [30,31], and the Arg guanidinium group would prefer to exit the lipid bilayer rather than to release a proton [21]. In the case of histidine, which is of particular interest for this work, the imidazole side chain has shown a pH sensitivity in the GWALP23 helix framework. When located at the center of the helix, the protonation of residue H12 drives the helix to the membrane surface, whereas residue H14 responds with modification of the helix tilt angle [32].

To further analyze the significance of the histidine side chain and its ionization behavior with respect to protein-lipid interactions, we have incorporated a pair of histidine residues at positions 8 and 16 within the hydrophobic core of GWALP23, but not adjacent to each other and not at the center of the helix. Rather, the two His residues are partially buried and are equidistant from the center of the helix. Residues H8 and H16 also are closer to each other than double histidine mutants of GWALP23 reported previously [34]. It is of interest also that positions 8 and 16 were previously examined with arginine residues [35]. The aim now is to compare the changes in helix orientation induced by the double histidine as opposed to double arginine replacements at positions 8 and 16 in GWALP23. Additionally, for better understanding of the behavior of GWALP23-H<sup>8,16</sup>, additional peptides with only one histidine at position 8 or position 16, namely GWALP23-H<sup>8</sup> and GWALP23-H<sup>16</sup>, also will be reported here. Analysis and comparison of the biophysical properties of these related peptides will provide deeper understanding of the principal effects of one or two buried histidine residues as well as their ionization properties for the interaction of a hydrophobic  $\alpha$ -helix with lipid bilayer membranes.

## 2. Materials and methods

The designed peptides were synthesized on a model 433A solid-phase peptide synthesizer (Applied Biosystems, from Life Technologies (Foster City, CA)) using a modified FastMoc™ chemistry on a 0.1-mmol scale, with extended times for deprotection or coupling where needed. Prior to synthesis, commercial L-alanine-d₄ (Cambridge Isotope Laboratories, Andover, MA) was Fmoc-protected using Fmoc-ON-succinimide, as described [36,37]. Other N-Fmoc amino acids and rink amide resins were purchased from NovaBiochem (San Diego, Ca), Anaspec (Fremont, CA) and Bachem (Torrence, CA). Histidine and tryptophan side chains were additionally protected with trityl and t-butoxycarbonyl protecting groups. For each peptide synthesis, typically two deuterium-labeled alanines with 50% and 100% isotope abundance were incorpo-

rated to help with the  $^2H$  spectral assignments. Signal intensity can decrease as  $|\Delta\nu_{\rm q}|$  increases and furthermore is sensitive to motions [38,39]. When necessary, peak assignments were confirmed by omitting a particular data point in a test calculation.

Synthesized peptides were cleaved from resin using a cleavage cocktail of 85:5:55 mixture of trifluoroacetic acid:phenol:triisopropylsi-lane:water at 22 °C for 2 h. After filtering off the resin support and precipitation of free peptides, purification of crude peptides was performed be means of reversed-phase HPLC. A Zorbax SB-C8 column (9.4  $\times$  250 mm) packed with 3.5  $\mu m$  octyl-silica from Agilent Technologies (Santa Clara, CA) was used for purification, with an elution gradient of 90–98% methanol (with 0.1% trifluoroacetic acid) over 40 min. The purified peptides were quantified using UV–Vis spectroscopy to measure the absorbance of Trp residues at 280 nm [40]. MALDI-TOF analysis was used for to verify the peptide molecular mass and extent of deuteration.

Oriented samples for solid-state NMR experiments were prepared mechanically on thin glass slides as described previously [41], with 1:60 peptide:lipid (mol:mol) ratio. The DLPC, DMPC, DPoPC and DOPC lipids from Avanti Polar Lipids (Alabaster, AL) were used to form the bilayer membranes. Peptide/lipid films were deposited on the slides from 95% methanol, dried under vacuum ( $10^{-4}$  Torr for 48 h), and hydrated (45% w/w) with deuterium-depleted water (Cambridge Isotope Laboratories, Andover, MA) containing 20 mM glycine or citrate buffer at a specific pH value between 2 and 8 [32,31]. The hydrated slides were stacked in 8 mm cuvettes, sealed with epoxy and incubated at 40 °C for at least 48 h to enable bilayer alignment.

Solid-state NMR spectra for  $^{31}P$  nuclei (for confirming the alignment of phosphate head groups in lipid bilayers) and  $^{2}H$  nuclei (for analysis of peptide orientations and dynamics based on  $^{2}H$ -labeled alanines in the peptide) were recorded using a Bruker Avance 300 spectrometer (Billerica, MA). The  $^{31}P$  NMR spectra were recorded in a Doty 8 mm wide line probe (Doty Scientific Inc., Columbia, SC) with broadband  $^{1}H$  decoupling on a Bruker Avance 300 spectrometer at both  $\beta=0^{\circ}$  (bilayer normal parallel to magnetic field) and  $\beta=90^{\circ}$  (bilayer normal perpendicular to magnetic field) macroscopic sample orientations. Before Fourier transformation, an exponential weighting function with 100 Hz line broadening was applied. The chemical shift was referenced externally to 85% phosphoric acid at 0 ppm.

The  $^2H$  NMR spectra were recorded at 50 °C with macroscopic sample orientations of  $\beta=90^\circ$  and  $\beta=0^\circ$ . A quadrupolar echo pulse sequence [42] was employed with full phase cycling, a pulse length of 3.2  $\mu s$ , echo delay of 105  $\mu s$  and a 120-ms recycle delay. Between 0.7 and one million free induction decays were accumulated during each  $^2H$  experiment. Fourier transformation was accomplished after applying an exponential weighting function with 100 Hz line broadening.

Samples for circular dichroism spectroscopy were prepared by forming small lipid vesicles incorporating 0.063  $\mu mol$  peptide and 3.75  $\mu mol$  lipid (1/60 peptide:lipid) using ultrasonication in unbuffered water. The peptide concentrations were determined by UV–Vis spectroscopy using a molar extinction coefficient for Trp at 280 nm of 5600  $M^{-1}$  cm $^{-1}$ . An average of ten scans was recorded on a Jasco J-1500 spectropolarimeter, using a 1 mm cell path length, 1.0 nm bandwidth, 0.1 nm slit and a scan speed of 20 nm/min.

Helix orientation and dynamics were analyzed using two methods, a semi-static Geometric Analysis of Labeled Alanines ("GALA") [41] and a modified Gaussian approach [28,43,44] for fitting the  $^2H$  NMR signals from the  $C_{\beta}D_3$  groups of Ala-d $_4$  residues. A  $C_{\alpha}$  deuteron also is present and has been observed in some samples [22,31], although the  $C_{\alpha}\text{-D}$  was not detected here. The measured  $C_{\beta}D_3$  quadrupolar splittings were estimated to 0.1 kHz and were reproducible to  $\pm 1$  kHz with duplicate samples. The  $^2H$  methods are complementary to  $^{15}N$  based methods for revealing helix orientations; the  $^2H$  and  $^{15}N$  methods also can be used in combination for characterization of membrane helices

[45,39,29,46]. For cases where alanine A7 did not fit the core helix (see Results section), the <sup>2</sup>H quadrupolar splitting for A7 was not included in either method of analysis. The GALA method uses the quadrupolar splitting values from <sup>2</sup>H-NMR spectra and fits a principal order parameter  $S_{zz}$ , an average helix tilt magnitude  $\tau_0$  and the direction of tilt also known as helix azimuthal rotation ( $\rho_0$ ), while maintaining an  $\epsilon_{\parallel}$  angle between the alanine  $C_{\alpha}$ – $C_{\beta}$  bond vector and the helix axis fixed at 59.4° [41]. The modified Gaussian approach involves three variable parameters, an average helix tilt  $\tau_0$ , mean azimuthal rotation  $\rho_0$  and rotational slippage  $\sigma_{\rho}$ , with fixed values for  $S_{zz}$  and  $\sigma_{\tau}$  (helix wobble) following [44]. Fixing a value for  $\sigma_{\tau}$  reduces the number of variables when considering limited data sets. It has been well established that  $\sigma_0$  is more important than  $\sigma_{\tau}$  for describing the dynamic properties of individual membrane helices [29,43,44]. Nevertheless, the appropriate range for  $\sigma_{\tau}$  may differ between transmembrane and surface helix orientations (see Results section). For transmembrane orientations, therefore, we maintained  $\sigma_{\tau}$  at 10°; but because this value would not fit the surface orientations, we maintained  $\sigma_{\tau}$  of 25° or 35° for the surface orientations, as validated previously by Lipinski et al. [35]. Other examples of model peptides having  $\sigma_{\tau}$  near 25° have been noted [47,48] (see Discussion section).

#### 3. Results

The indicated peptides (Table 1; Fig. 1) were successfully synthesized and characterized. The MALDI-TOF mass spectra of GWALP23-H<sup>8,16</sup> and GWALP23-H<sup>8</sup> (Fig. S1 of the Supporting Information) confirm the expected molecular masses and isotope distributions for labeled peptides with full or partial deuteration of two alanines. The CD spectra are characteristic of  $\alpha$ -helices in DLPC, DMPC and DOPC lipid vesicles, with a distinct minimum at 208 nm and a broad shoulder around 222 nm (Fig. S2). The alignment of lipid molecules in the bilayers with the incorporated peptides has been assessed and confirmed by means of  $^{31}\text{P}$  NMR spectroscopy (Figs. S3, S4, S5). We will present solid-state  $^2\text{H}$  NMR results that reveal the helix orientations and pH dependence for bilayer-peptide samples when a single His residue is present and then will compare the properties when histidines H8 and H16 are present together.

# 3.1. GWALP23-H<sup>8</sup> and GWALP23-H<sup>16</sup> individually

To examine the influence of one particular His residue, we incorporated histidine instead of leucine at position 8 or 16 to give the resulting single-His mutants of the parent GWALP23 peptide, namely  $\rm GWALP23-H^8$  or  $\rm GWALP23-H^{16}$  (Table 1). The orientations and titration behavior of the resulting helices were examined in bilayer membranes.

Table 1
Sequences of buried single and paired histidine and arginine mutants of GWALP23 peptides.

Name of peptide	Sequence	Reference
GWALP23 GWALP23-H <sup>8</sup>	Acetyl-GGALWLALALALALALALWLAGA-amide Acetyl-GGALWLAH <sup>8</sup> ALALALALALWLAGA-amide	[71] This work
GWALP23-H <sup>16</sup>	Acetyl-GGALWLALALALALAH <sup>16</sup> ALWLAGA-amide	This work
GWALP23-H <sup>8,16</sup>	Acetyl-GGALWLAH <sup>8</sup> ALALALAH <sup>16</sup> ALWLAGA- amide	This work
GWALP23-R <sup>8,16</sup>	Acetyl-GGALWLAR $^8\mathrm{ALALALAR}$ $^{16}\mathrm{ALWLAGA-amide}$	[35]

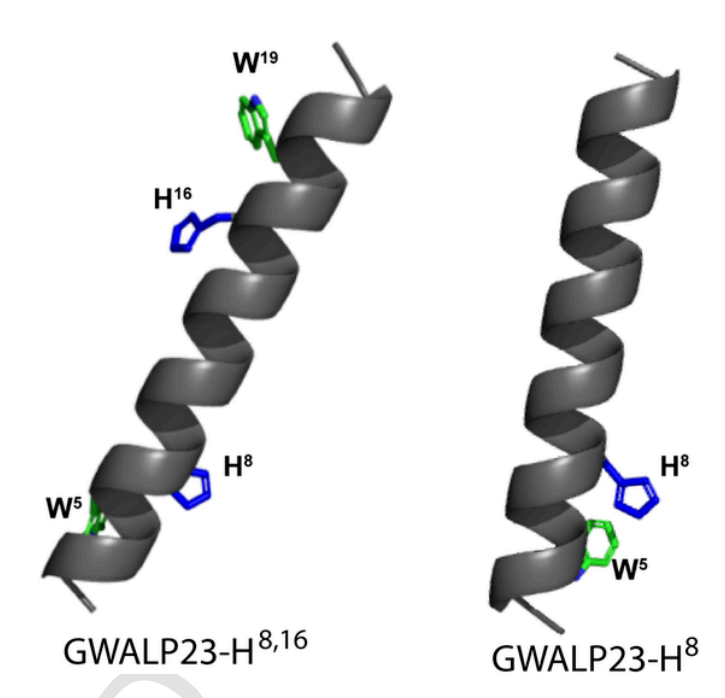


Fig. 1. Models to illustrate the positions of histidine residues introduced within the helix of GWALP23 and the orientations of two peptides relative to a vertical bilayer normal in DLPC lipid bilayers, drawn using Pymol [69].

## 3.2. <sup>2</sup>H NMR in thinner DLPC and DMPC bilayer membranes

The  $^2H$  NMR spectra for the aligned samples of GWALP23-H $^8$  reveal well-defined signals and distinct quadrupolar splittings of core Ala residues in lipid bilayers of DLPC and in DMPC at low pH (Fig. 2). Interestingly, the signals change with pH (see below). The spectra indicate single tilted transmembrane orientations except when the pH is raised in DMPC. The quadrupolar splitting magnitudes  $|\Delta\nu_{\rm q}|$  of GWALP23-H $^8$  range at pH 2 from about 2 kHz to 24 kHz in DLPC and 1.5 kHz to 23 kHz in DMPC. While the  $|\Delta\nu_{\rm q}|$  ranges are comparable to those of the parent GWALP23, suggesting well aligned helices, the radial distribution of values changes dramatically when H8 is introduced. For example,  $|\Delta\nu_{\rm q}|$  for alanine A7 changes from 26 kHz (DLPC) and 22 kHz (DMPC) to 1 or 2 kHz in each lipid (Table 2), indicating large differences in the azimuthal rotation of the tilted helix with H8.

The helix tilt analysis using either the semi-static GALA or the Gaussian analysis reveals similar orientations with similar tilt angles of  $10{\text -}12^\circ$  for the GWALP23-H $^8$  helix in DLPC and DMPC (Table 3; Fig. 3). Compared to the parent GWALP23 helix, GWALP23-H $^8$  displays a large rotational difference  $\Delta\rho$  of  $150^\circ$  about the helix axis and loses the sensitivity of tilt angle to bilayer thickness (Table 3). Indeed, the observed azimuthal rotation  $\rho_0$  for GWALP23 in DLPC and DMPC is about  $305^\circ$  –  $311^\circ$ , compared to  $155^\circ$  –  $160^\circ$  for GWALP-H $^8$ . The modified Gaussian analysis shows agreement, with similar values of  $\tau_0$  and  $\rho_0$  and only a moderate rotational slippage  $\sigma_\rho$  of about  $40^\circ$ .

## 3.3. <sup>2</sup>H NMR in thicker and unsaturated DOPC lipid membranes

In the case of GWALP23-H<sup>8</sup>, as the acyl chain length and bilayer thickness increase from DLPC to DOPC at neutral pH, there is a distinct decrease in spectral quality. The spectra become characterized by poor signal-to-noise ratio where individual quadrupolar splittings are no longer distinguishable (Fig. 4); rather the multiple overlapped signals give rise to broad peaks for each labeled alanine in DOPC, suggesting

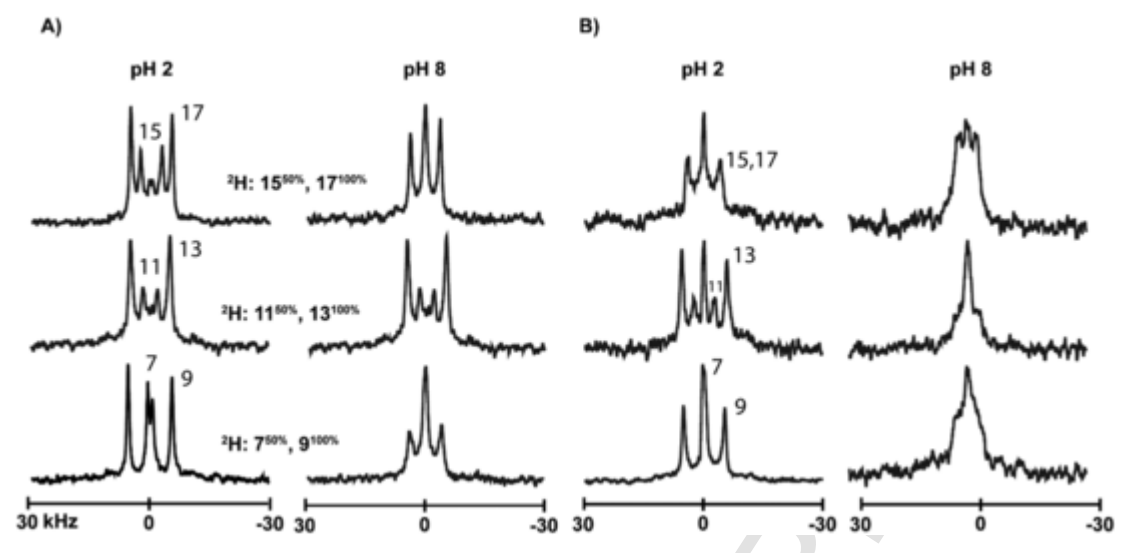


Fig. 2.  $^2$ H NMR spectra of labeled alanines in the GWALP23-H $^8$  core helix in DLPC (A) and DMPC (B) bilayer membranes at pH 2 and pH 8. Sample orientation is  $\beta = 90^\circ$ , 1:60 peptide:lipid at 50  $^\circ$ C. The changes in quadrupolar splittings in DLPC and spectral quality in DMPC indicate the response of the helix to the change in ionization state of histidine H8. Levels of deuteration, Ala identities and representative peak assignments are indicated.

Peptide	ptide Lipid pH Ala ${ m CD_3}$ quadrupolar splittings $^{\circ}$									
			A7	A9	A11	A13	A15	A17		
GWALP23	DLPC		26.4	25.5	26.9	14.6	20.7	3.4		
	DMPC		21.9	8.9	20.9	3.8	17.6	2.9		
	DOPC		16.6	1.7	16.7	1.5	15.4	2.6		
H 8	DLPC	2	2.2	22.2	11.7	24.0	10.7	21.1		
		8	2.3	16.1	7.5	19.7	2.2	15.2		
	DMPC	2	1.4	20.7	10.7	23.0	8.3	16.8		
		8 b	1, 13		3, 14		2, 9	2, 9		
	DOPC	8 <sup>b</sup>	2, 7, 14, 20		7, 11, 20, 23		2, 6, 1	2, 6, 12, 16		
H 16	DOPC	2	5.8	19.6	3.2	14.4	7.2	5.2		
		6	0.6	12.8	1.0	9.6	8.4	3.8		
H 8,16	DLPC	4	33.7	33.7	30.2	29.8	8.4	18.5		
	DMPC <sup>c</sup> (major)		28.4	29.2	24.6	25.8		-		
	DMPC (minor)		24	24	16.2	1.8	-	_		
	DPoPC		24.1	24.0	16.1	1.7	13.7	29.0		
	DOPC		22.3	23.8	16.0	1.4	13.4	31.2		

 $<sup>^</sup>a$  Values are reported for  $\beta=0\,^o$  sample orientations. The experimental uncertainty is about  $\pm 1$  kHz. The GWALP23 samples were unbuffered at neutral pH.

multi-state behavior or perhaps a distribution of orientations around an average  $\tau_0$  [49,50]. Due to a high noise level in the spectra of the DOPC samples that complicates the individual assignments of quadrupolar splittings, the  $|\Delta\nu_q|$  magnitudes listed in Table 2 for the DOPC experiments are approximate. For the same reason, the GALA quadrupolar wave plot for GWALP23-H<sup>8</sup> in DOPC cannot be constructed at this time.

Considering now GWALP23- $\mathrm{H}^{16}$ , the multi-state behavior is not observed in DOPC. Rather, distinct individual  $^{2}\mathrm{H}$  resonances are observed

for the labeled core alanines (Fig. S6 of the Supporting Information), and a tilt angle of about  $6^{\circ}$  –  $8^{\circ}$  from the bilayer normal can be deduced for the transmembrane helix (Table 3; Fig. 3C). The tilt of GWALP23-H<sup>16</sup> indeed is distinct from that of GWALP23 and previously characterized single mutants having H12 or H14 [32]. A pH dependence of the tilt angle also can be measured (see below). Notably, the helix with H16 shows a single transmembrane state that can be titrated, whereas the helix with H8 occupies a distribution of states in DOPC.

## 3.4. Individual titrations of H8 and H16

Because the sequences of GWALP-H<sup>8</sup> and GWALP-H<sup>16</sup> contain only single ionizable residues, changes in the  $^2\text{H}$  NMR spectra might enable estimation of the titration point of H8 or H16 in a membrane environment. The  $^2\text{H}$  NMR spectra of GWALP23-H<sup>8</sup> under pH conditions from acidic to basic are shown in Fig. 5 and supplementary Fig. S7. In DLPC, the spectral quality remains unchanged from pH 2 to pH 8 while the methyl  $^2\text{H}$  quadrupolar splittings of A11 and A13 decrease from about 12 kHz to 7.5 kHz, and 24 kHz to 20 kHz, respectively (Table 2). Using the  $|\Delta\nu_q|$  values over a pH range from 2 to 8, titration curves are obtained for A11 and A13 in DLPC (Fig. 6A). Although the plateau levels at low pH are not entirely established, both curves show midpoints at about pH 3.6, indicating an upper limit of 3.6 for the pKa of the H8 imidazole side chain in DLPC.

In DMPC, there are additional spectral changes, including changes in the quadrupolar splittings. In an acidic environment, from pH 2 to pH 4, the signals from the  $^2\text{H}\text{-}Ala$  labels of GWALP-H8 are well resolved with noticeable movement of the peaks for labeled A11 and A13, resulting from changes in quadrupolar splitting values. As the sample pH is raised incrementally from 4 to 8, there is then a progressive decrease in spectral quality leading to overlapping of the primary peaks (Fig. 5). To confirm these changes between pH 2 and pH 8, samples with other  $^2\text{H}\text{-}labeled$  core alanines were also hydrated with pH 8 buffer, and similar poorly resolved spectra were observed at pH 8 in each case (Fig. 2B, rightmost panel). These results confirm the deprotonation of H8 side chain in DMPC when the pH is in the basic range. Plotting the  $|\Delta\nu_q|$  values of A11 and A13 versus pH in DMPC, an upper limit of about 3.2 is estimated for the pKa of the H8 imidazole ring in DMPC bilayers (Fig. 6), similar to that observed in DLPC.

As noted above,  $GWALP23-H^8$  occupies multiple states in DOPC bilayers, states which cannot yet be assigned. Unfortunately, the distribu-

 $<sup>^</sup>b$  Since multiple weak and overlapped signals are observed for each double-labeled sample, it was not possible to assign the exact  $|\Delta\nu_q|$  values for GWALP23-H  $^8$  in DMPC or DOPC lipids at pH 8.

 $<sup>^</sup>c$  The signals from labeled alanines of GWALP23-H  $^{8,16}$  in DMPC display multiple broad and overlapped signals. To address the  $\Delta\nu_q$  values, we have reported here the average values of overlapped signals. The assignments for A15 and A17 in DMPC were not possible to retrieve due to a poor signal to noise ratio.

**Table 3**Semi-static GALA and Modified Gaussian analysis results for GWALP23-H <sup>8,16</sup> and GWALP23-H <sup>8</sup> helices in lipid bilayers.

Peptide	Lipid	pН	Semi-static				Modified Gaussian				Ref	
			$\tau_0$	ρο	$S_{zz}$	RMSD	$\tau_0$	ρο	$\sigma_{ au}$	$\sigma_{\rho}$	RMSD	
GWALP23	DLPC	_ a	20.7°	305°	0.66	0.71	23°	304°	15°	33°	0.7	[70,44]
	DMPC	_	9.0°	311°	0.89	1.06	13°	308°	10°	42°	1.19	
	DOPC	-	6.0°	323°	0.87	0.57	9°	321°	9°	48°	0.7	
H 8	DLPC	2	11.7°	160°	0.85	0.23	15°	160°	10°	38°	0.48	This work
		8	8.7°	148°	0.77	1.20	8°	144°	10°	0°	1.03	
	DMPC b	2	10.7°	156°	0.81	0.90	14°	156°	10°	42	0.98	
H <sup>16</sup>	DOPC	2	8.3°	101°	0.85	0.54	-	-	-	-	-	
		6	5.7°	90°	0.73	0.67	-	-	-	-	-	
H 8,16	DLPC	4	25.0°	122°	0.82	1.06	29°	122°	10°	28°	0.94	This work
	DMPC (major)	4	21.7°	116°	0.8	1.15						
	DMPC (minor)	4	87°	31°	0.57	0.76						
	DPoPC	4	87.3°	32°	0.54	0.76	84°	$28^{\circ}$	35°	16°	1.45	
	DOPC	4	87.6°	32°	0.55	0.82	83°	28°	35°	16°	1.18	

<sup>&</sup>lt;sup>a</sup> The GWALP23 samples were unbuffered at neutral pH.

tion of states in DOPC persists when the pH is changed. GWALP23-H<sup>8</sup> continues to display weak resonances and remains multi-state or perhaps somewhat aggregated irrespective of the pH (Fig. S7). By contrast, GWALP23-H<sup>16</sup> occupies a single transmembrane state in DOPC (Fig. 3C), and this state can be titrated. When the pH is lowered from 6 to 2, the His imidazole side chain becomes charged, and changes in  $|\Delta\nu_q|$  for the <sup>2</sup>H-methyl groups of core alanine residues, including A11 and A13, are observed (Fig. 7). Collectively, the changes observed in  $|\Delta\nu_q|$  reveal a well-defined orientation for GWALP23-H<sup>16</sup> at low pH and a different orientation when the pH is raised to 6 (Fig. 3C). The changes in  $|\Delta\nu_q|$  for residues A11 and A13 reveal titration curves for GWALP23-H<sup>16</sup> in DOPC bilayers (Fig. 6C), indicating an upper limit of about 3.5 for pKa of the H16 side chain.

As the quadrupolar splittings for GWALP23-H<sup>8</sup> change with pH in DLPC and DMPC membranes, it is reasonable that the orientation of this helix also may change with pH. The GALA analysis results for GWALP23-H<sup>8</sup> at pH 2 and pH 8 (Table 3) and the quadrupolar wave plots (Fig. 3) confirm the changes. The GWALP23-H<sup>8</sup> helix in DLPC is found to decrease its tilt by about 3° with no significant change in the azimuthal rotation when the pH is raised from 2 to 8. In DMPC, because of the overlapping of signals, the orientation of GWALP23-H<sup>8</sup> could be determined only when H8 is charged at low pH (Fig. 3B). When H8 is positively charged, the helix orientation is similar in DLPC and DMPC (Table 3). When H8 is neutral, the helix adopts a distribution of states in DMPC, similar to its status in DOPC at all pH values; these states cannot yet be defined. Notably, the titration of H16 changes the tilt of the GWALP23-H<sup>16</sup> helix in DOPC by about 3° and the azimuthal rotation by about 10° (Table 3).

# 3.5. GWALP23-H<sup>8,16</sup>

## 3.5.1. Helix properties in thinner DLPC and thicker DOPC membranes

When H8 and H16 both are present, the solid-state  $^2H$  NMR spectra of aligned samples display distinct signals for each  $^2H$ -labeled side-chain methyl group of alanine residues 7, 9, 11, 13, 15 and 17 in DLPC and DOPC lipid bilayers (Fig. 8). The quadrupolar splittings ( $|\Delta\nu_q|$ ) span ranges that are quite large, 8–34 kHz in DLPC and 1–24 kHz in DOPC, indicating good helix alignment and some possible changes in helix orientation as a function of bilayer thickness (Table 2). Notably,

the  $^2H$  labels on the Ala residues next to H8 and H16, namely A7, A9, A15 and A17, produce sharp and distinct resonances. Further analysis by the semi-static GALA method reveals dramatically different helix orientation with respect to DLPC and DOPC membranes (Table 3; Fig. 9). In DLPC, the helix of GWALP23-H<sup>8,16</sup> resides in the membrane as a transmembrane helix with a mean tilt angle  $(\tau_0)$  of  $\sim\!25^\circ$  from the bilayer normal. Interestingly, the helix assumes an orientation on the surface of DOPC membranes (Fig. 9B), where the helix tilt  $(\tau_0)$  is about 87° from the bilayer normal (Table 3). Importantly, the experimental DLPC and DOPC membranes are both in the liquid-crystalline phase. Residue A7 fails to fit the quadrupolar wave for the surface helix on DOPC (Fig. 9B), as  $|\Delta\nu_{\rm q}|$  deviates by about 5.4 kHz (compared to an experimental uncertainty of about 1 kHz). This deviation suggests that residues 1–7 miss the helical geometry and thereby are unraveled from the surface-bound core helix

To confirm these results, we employed a modified Gaussian analysis, described previously [28,44], to fit the average tilt and rotation  $\tau_0$  and  $\rho_0$ , and the azimuthal slippage  $\sigma_\rho$  about the helix axis. This analysis agrees with the results for GWALP23-H<sup>8,16</sup> in DLPC and DOPC membranes, by showing similar values of  $\tau_0$  and  $\rho_0$  as those derived from the GALA analysis (Table 3). Importantly, the surface orientation with respect to DOPC bilayers also is confirmed by the modified Gaussian analysis. Notably, the rotational slippage  $\sigma_\rho$  remains always low, and is even lower for the surface orientation (Table 3). Because of the very different helix orientations with respect to DLPC and DOPC, we investigated the GWALP23-H<sup>8,16</sup> helix also in bilayers of intermediate thickness

## 3.5.2. Helix properties in intermediate-thickness DMPC and DPoPC bilayers

In contrast to the well-defined individual <sup>2</sup>H quadrupolar splittings observed in the spectra from helices of GWALP23-H<sup>8,16</sup> in DLPC and DOPC bilayers, in DMPC the <sup>2</sup>H NMR spectra from the labeled core alanines are poorly resolved and display multiple resonances for each Ala residue (Fig. 8). Notably, the acyl chains of DMPC have hydrophobic length of about 24.8 Å, intermediate between the lengths of DLPC (20.8 Å) and DOPC (26.2 Å) acyl chains [51,52]. The peptide core helix spans 1.5 Å per residue, namely about 22 Å from W5 to W19, but only about 13 Å from H8 to H16. Although a transmembrane helix of GWALP23-H<sup>8,16</sup> spans a DLPC bilayer, the multiple low-intensity broad

b Since the individual quadrupolar splitting values for GWALP23-H 8 in DMPC at pH 8 and in DOPC were not possible to retrieve, GALA analysis was not performed for these cases.

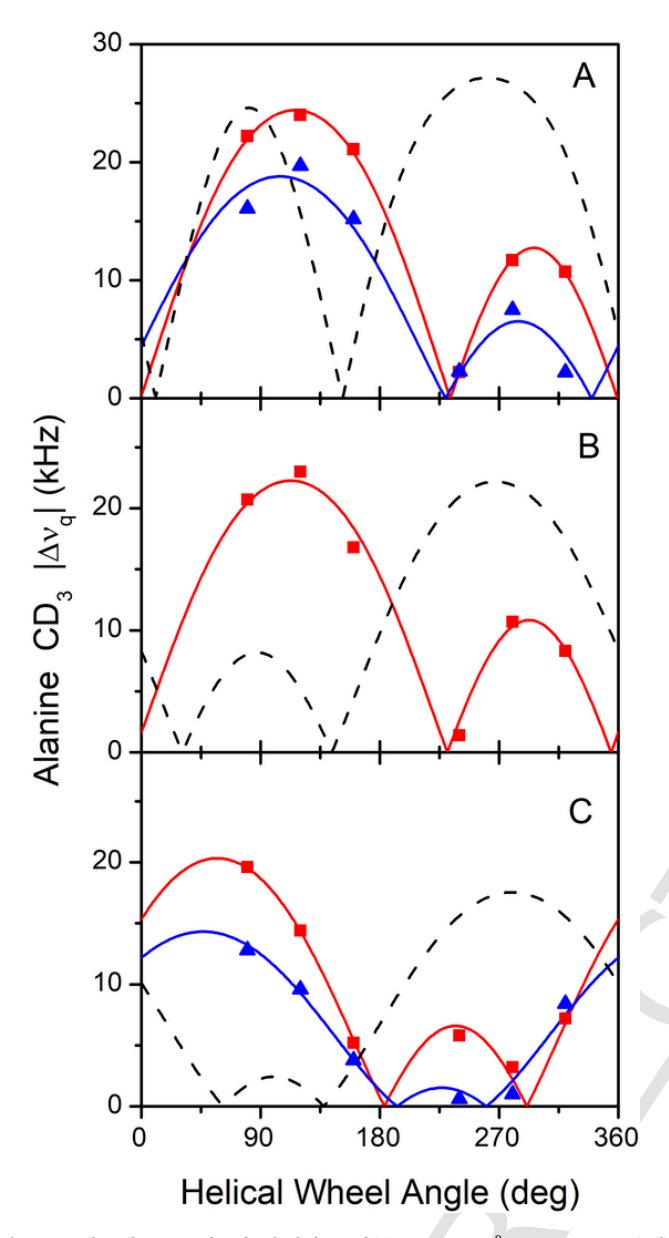
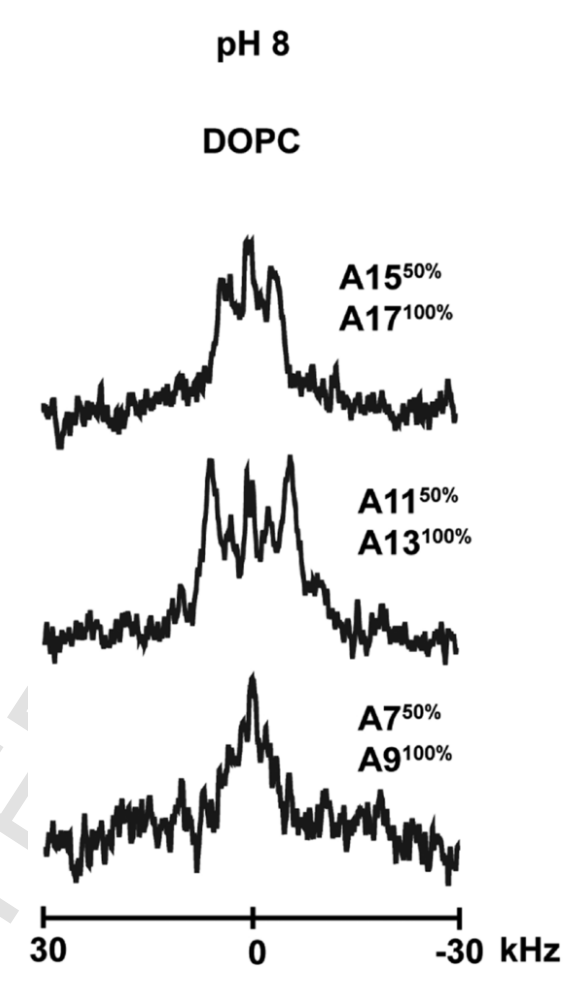


Fig. 3. Quadrupolar wave plots for the helices of (A) GWALP23-H $^8$  in DLPC at pH 2 (red) and pH 8 (blue), (B) GWALP23-H $^8$  in DMPC at pH 2 (red), and (C) GWALP23-H $^{16}$  in DOPC at pH 2 (red) and pH 6 (blue). Reference curves are shown (dotted black curves) for the orientation of the parent GWALP23 in each lipid helix at neutral pH (from ref. [70]). At high pH, with a midpoint of 3.2 (see Fig. 10), the GWALP23-H $^8$  helix transitions to multiple states in DMPC, so a single helix orientation cannot yet be determined. (For interpretation of the references to colour in this figure legend, the reader is referred to the web version of this article.)

peaks NMR for GWALP23-H<sup>8,16</sup> in DMPC suggest two or more states for the peptide helix with respect to the lipid bilayer membrane, in slow exchange on the NMR time scale. By measuring the quadrupolar splitting for each signal, one deduces two distinct sets of these magnitudes for the set of alanine labels. One set of quadrupolar splittings matches closely with the signals observed in DLPC, while the other set overlaps closely with the signals from DOPC (Table 2). Due to a low signal to noise ratio, we could not resolve the quadrupolar splitting values for A15 and A17 in DMPC. For this reason, we performed semi-static GALA analysis using only the signals from alanines 7, 9, 11 and 13.

The semi-static GALA analysis reveals two orientations of the GWALP23-H<sup>8,16</sup> helix in DMPC membranes. One state is a transmembrane orientation with a tilt ( $\tau_0$ ) of ~22°, slightly lower than the tilt in



**Fig. 4.** <sup>2</sup>H NMR spectra of labeled alanines in the GWALP23-H<sup>8</sup> core helix at pH 8 in DOPC lipid bilayers. Multiple peaks are observed for each labeled alanine. Sample orientation is  $\beta = 90^{\circ}$ , 1:60 peptide:lipid at 50 °C.

DLPC, while the other orientation is surface bound similar to that found on the surface of DOPC membranes (Fig. 10, Table 3). The azimuthal rotation ( $\rho_0$ ) for the surface helix remains remarkably similar to the orientation on DOPC membranes. For the transmembrane orientation, the helix azimuthal rotation ( $\rho_0$ ) differs by only about 5° from that observed in DLPC. Since the signal intensity for transmembrane orientation predominates somewhat (although not tremendously) over that for the surface orientation, we note that slightly more than half of the peptide helix population adopts the transmembrane orientation in DMPC, while a significant minority population leaves the membrane and embraces a surface orientation (Fig. 10).

For comparison with results in the 14-carbon and 18-carbon acyl-chain DMPC and DOPC bilayers, we performed NMR experiments with samples in oriented DPoPC bilayers. From the <sup>2</sup>H NMR spectra of helices in this 16-carbon unsaturated acyl-chain DPoPC lipid environment, it is evident that GWALP23-H<sup>8,16</sup> exhibits one major set of distinct pairs of signals for the CD<sub>3</sub> methyl side chains of all six core alanines (Fig. 8), with quadrupolar splittings almost identical to those observed for experiments in DOPC (Table 2). Nevertheless, the spectral quality is not as well resolved as for the DOPC spectra, although the resonances are prominent and overlap closely with the DOPC signals (Fig. 8). Interestingly, there are a few additional signals with very low intensity, whose quadrupolar splitting values are similar those from the transmembrane helix in DMPC and DLPC. The minor peaks indicate the existence of a minor membrane-embedded population of the helix in DPoPC. Further orientational analysis confirms that the major orienta-

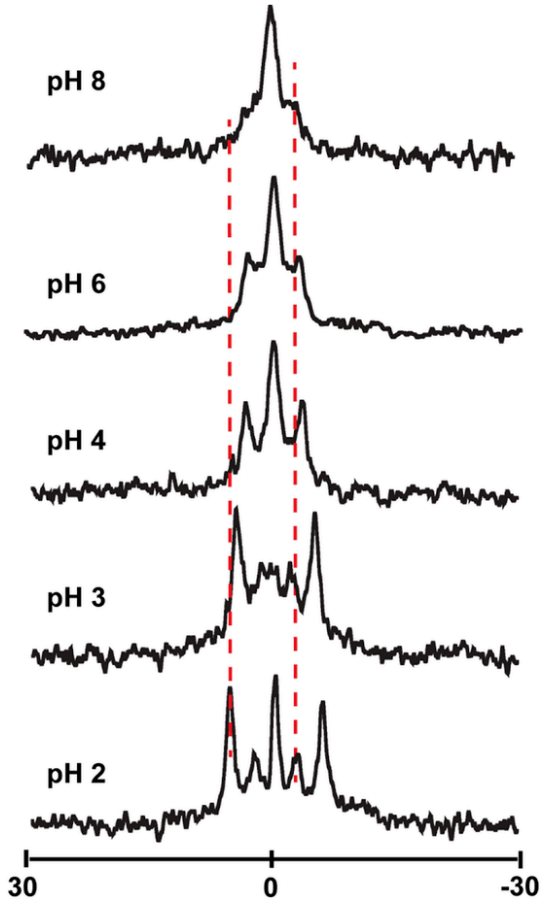


Fig. 5. Selected  $^2H$  NMR spectra for deuterated alanines A11 and A13 of GWALP23-H<sup>8</sup> in DMPC hydrated with 20 mM buffer at the indicated pH values. Sample orientation is  $\beta=90^\circ, 1:60$  peptide:lipid at 50  $^\circ$ C.

tion of GWALP23-H<sup>8,16</sup> on DPoPC bilayers is surface bound, as shown by the quadrupolar wave plot in Fig. 9B, with identical  $\tau_0$  and  $\rho_0$  values as the surface population on DOPC membranes. Modified Gaussian analysis furthermore shows agreement with the semi-static GALA analysis (Table 3).

## 3.6. Titration of the H8 and H16 combination

To address pH dependence, oriented samples of GWALP23-H<sup>8,16</sup> with <sup>2</sup>H-labeles at A11 and A13 were prepared in bilayers of DOPC under acidic and basic conditions. Fig. 11 shows the spectra in DOPC lipid membranes hydrated with buffers having pH from 2 to 8. Quadrupolar splittings and overall spectral quality remain universally unchanged over this pH range (Fig. 11), indicating no change in the orientation of the GWALP23-H<sup>8,16</sup> peptide helix, whether or not the ionization of histidine side chains changes over this range of pH. These experiments were performed also in DLPC and DMPC lipid membranes where, once again, no noticeable changes were observed in either membrane (Fig. 11). In DMPC the peptide continues to display multiple signals irrespective of pH, with almost no changes in the positions of peaks or signal intensities. These results involving no pH dependency in the peptide orientations are consistent with other double histidine peptides, including  $\mbox{GWALP23-H}^{12,16}$  and  $\mbox{GWALP23-H}^{12,14}$  [53], involving histidines partially buried in the hydrophobic membrane, as well as H<sup>2,22</sup>WALP23 and  $GH^{5,19}ALP23$  [34], where the histidines are located at the membrane interface.

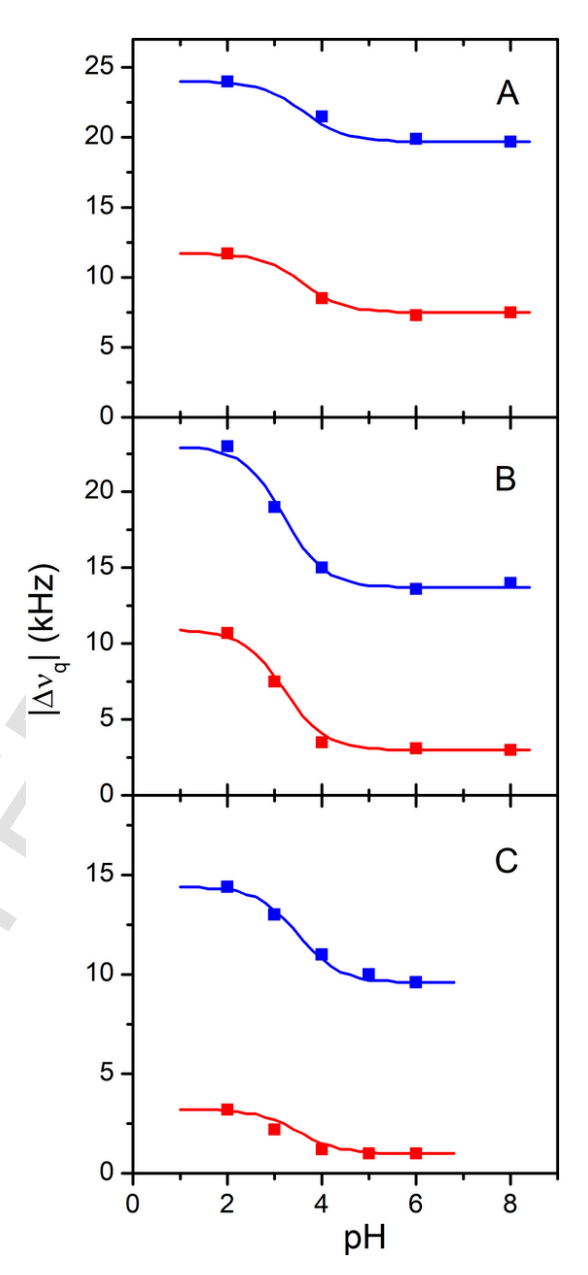


Fig. 6. Plots indicating the histidine titration for H8 in GWALP23-H<sup>8</sup> in DLPC (A) and DMPC (B) bilayer membranes. Graph (C) shows the titration for H16 in GWALP23-H<sup>16</sup> in DOPC. The curves for the  $|\Delta v_q|$  magnitudes for the CD<sub>3</sub> groups of A11 (red) and A13 (blue) in each graph indicate similar pKa values of about 3.6, 3.2 and 3.5, in graphs A, B and C, respectively. (For interpretation of the references to colour in this figure legend, the reader is referred to the web version of this article.)

## 4. Discussion

We have addressed questions of how the relative positions of one or two histidine residues within or near the central hydrophobic region of a lipid-bilayer membrane affect the orientation and dynamics of a transmembrane helix. The now canonical  $\alpha\text{-helical}$  model transmembrane helix GWALP23 served as an initial "host" framework into which the "guest" histidine residues were introduced singly or as a pair, so that the influence of this aromatic and potentially positively charged residue could be evaluated. The effects of the His residues H8 and H16 will be considered and compared with the baseline properties of the host 23-residue transmembrane peptide helix itself, or with arginines R8 and R16.

F. Afrose et al. BBA - Biomembranes xxxx (xxxxx) xxxx-xxxx

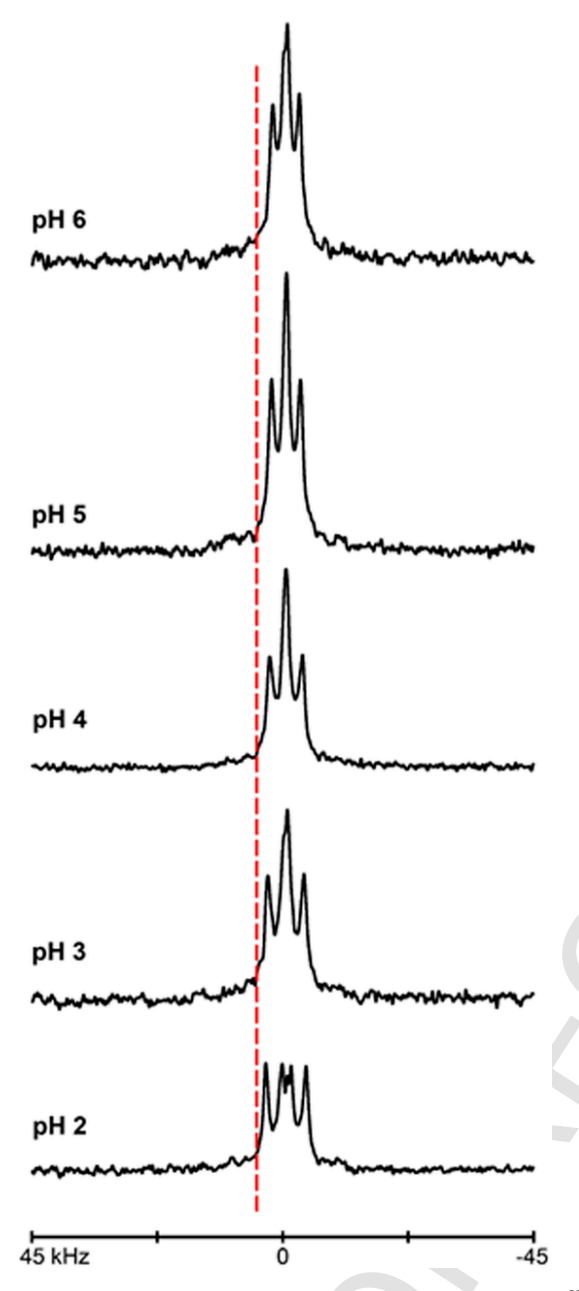


Fig. 7. Selected deuterium NMR spectra for labeled alanines 11 and 13 of GWALP<sup>23</sup>-H16 in DOPC bilayers, hydrated with 10 mM buffer at the indicated pH values. Sample orientation is  $\beta=90^{\circ}$ , 1:60 peptide:lipid at 50 °C.

In the modifications of GWALP23 considered here, the His residues at positions 8 and 16 are equidistant from the peptide center, with their  $\alpha\text{-carbons}$  displaced from each other by about 12 Å along the bilayer normal and by about 80° radially (Fig. 1). Notably, the helix is not symmetric yet rather proceeds from N-terminal to C-terminal. Positions 8 and 16 therefore experience different environments and may exhibit different interactions with lipids. Consequently, differing properties may be expected and are indeed observed for helices with H8 or H16 alone.

A previous study with mutations involving Arg residues at the same positions showed interesting results [35]. Because of the potential "snorkeling" of Arg side chains, the distance between the R8 and R16 guanidinium groups can increase and provide access of the side chains to the membrane-water interface. As a result, the 23-residue helix with R8 and R16 adopts transmembrane orientations in thinner membranes

such as DLPC and DMPC, while having a transition state in thicker DOPC bilayers, where the major orientation is surface bound and a minor orientation is transmembrane. The minor transmembrane orientation then is completely absent when GWALP23-R<sup>8,16</sup> is transferred to DEiPC bilayers with 20-carbon acyl chains [35]. These results support the snorkeling behavior of Arg side chains, a concept introduced by others in earlier studies [54,55]. Similar snorkeling of lysine was also investigated [56]. Here, we have investigated whether histidine, with less steric flexibility than Lys or Arg, has similar ability to confer a bilayer thickness dependence to a transmembrane helix. Although the snorkeling effect may allow positively charged residues to be placed near the negatively-charged phospholipid head groups [54,56,57], the situation could be more complicated because the His side chain has a ring and not a flexible chain. Histidine furthermore can titrate with a pKa that typically is close to physiological pH in aqueous solution.

The results from the <sup>2</sup>H NMR spectroscopy reveal orientation transitions of GWALP23-H<sup>8,16</sup> that depend on the thicknesses of bilayer membranes. GWALP23-H<sup>8,16</sup> exhibits a tilted transmembrane orientation in DLPC with a tilt angle of about 25°, which is similar and slightly higher than that of GWALP23 (Table 3). With arginines at the same positions, the tilt of the GWALP23-R<sup>8,16</sup> helix  $(\tau_0)$  is even higher  $(29^\circ)$  [35]. Thus, the observed magnitude of tilt  $\tau_0$  is possibly tuned by the length of the positively-charged side chains of residues 8 and 16. Moreover, the aromaticity of histidine may play a role, rendering the side chain somewhat compatible with the hydrophobic region of the bilayer. In DMPC, the bilayer hydrophobic region increases by 4 Å to about 25 Å thickness [51,52]; hence H8 and H16 may fail to snorkel to the membrane-water interface. While some of the subtle details are unknown, the combined effects eventually lead to multiple orientations for the GWALP23-H<sup>8,16</sup> helix with respect to DMPC lipid bilayers. Although the major population remains oriented as a transmembrane helix, a significant fraction goes to the surface of DMPC bilayers (Figs. 9-10). Interestingly in the case of the arginine cousin, a similar transition happens in DOPC membranes as opposed to DMPC membranes [35]. Due to the length of the Arg side chain, GWALP23-R<sup>8,16</sup> preserves its membrane spanning orientation in DMPC, while histidines with shorter side chains fail to do so in the same membrane. Notably, when the helix of GWALP23-H<sup>8,16</sup> is moved to the comparatively thicker DPoPC or DOPC bilayers, the surface orientation dominates as the major population of the peptide (Figs.

Two other GWALP23 family peptides with pairs of histidine residues (with  $\mathrm{H}^{12,14}$  and  $\mathrm{H}^{12,16}$ ) display also such surface-bound orientations in DOPC. In each case, due to a failure to accommodate both histidine residues within the bilayer, the helices leave the membrane and prefer to sit close to the interface [53]. These peptides furthermore exhibit a common feature of a transmembrane orientation in the thinner DLPC bilayer. All of these results suggest that histidine may somewhat extend or "snorkel" its side chain, although to a lesser extent than lysine or arginine

To test for possible effects of histidine ionization in the two different helix orientations experienced by GWALP23-H<sup>8,16</sup>, we performed experiments with labeled A7 and A9 at acidic and basic pH. Interestingly, no changes in spectral quality or quadrupolar splittings were observed in any of the DLPC, DMPC or DOPC bilayer membranes between pH 2 and pH 8 (Fig. 11). Because the individual H8 and H16 residues are observed to titrate in the transmembrane helix (Figs. 5–7), the results are puzzling for the combined pair of His residues Regardless of pH, the GWALP23-H<sup>8,16</sup> helix persists as transmembrane in DLPC, multi-state in DMPC and surface-bound in DOPC. Now these results seem to agree with previous findings that several other pairs of bilayer-buried His residues lose the pH response [53], whereas single isolated histidines are sensitive to pH [32]. For helices with four histidines, a distinct transition from surface-bound (at low pH) to transmembrane (at high pH) has been noted to be possibly cooperative [16,58]. Never-

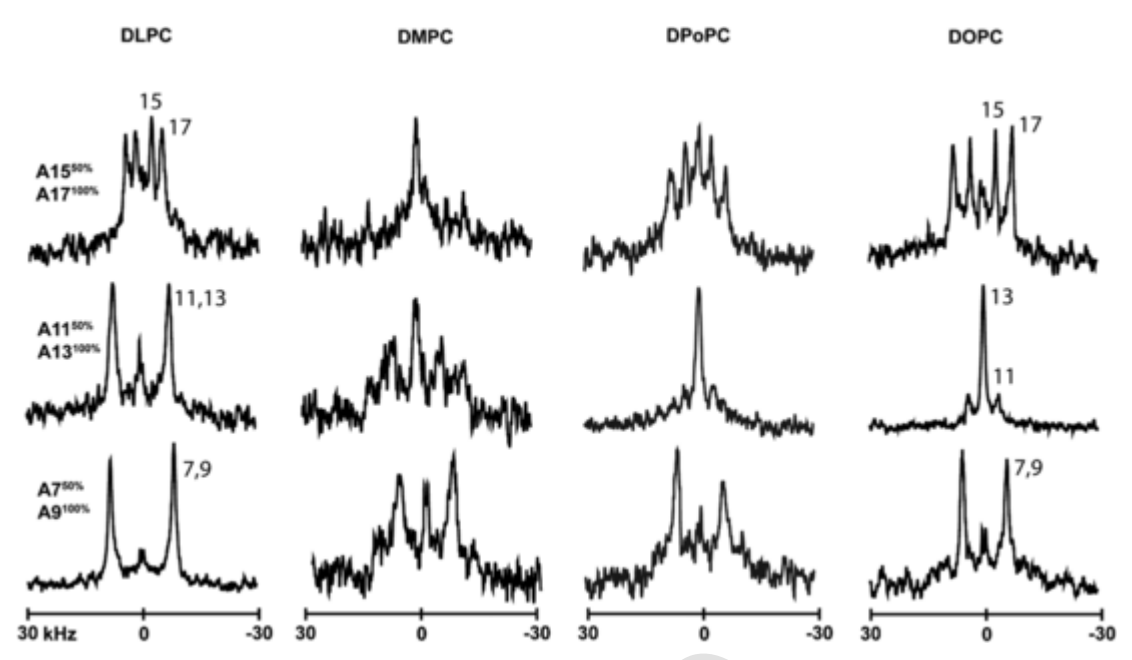


Fig. 8.  $^2$ H NMR spectra of labeled alanines in the GWALP23-H $^{8,16}$  core helix in DLPC, DMPC, DPoPC and DOPC lipid bilayers hydrated with 20 mM buffer at pH 4. Sample orientation is  $\beta = 90^{\circ}$ , 1:60 peptide:lipid at 50  $^{\circ}$ C. Levels of deuteration, Ala identities and representative peak assignments are indicated.

theless, the helix of GWALP23-H<sup>8,16</sup> tends to maintain the same bilayer-dependent orientation irrespective of pH. Notably, all interactions that favor or disfavor one orientation of a helix will come into play in each of the bilayer membranes [16,58], such that a pH dependence could be overridden by other factors.

An individual His residue greatly influences the rotational orientation of the transmembrane helix, with H8 changing  $\rho_0$  by  $150^\circ$  and H16 by  $210^\circ$  (Table 3). When H8 and H16 are present together, for the transmembrane population, the helix rotation assumes an intermediate value (Table 3) that is about  $170^\circ$  away from  $\rho_0$  for the helix with no histidines. The rotational changes about the helix axis likely optimize the interactions of the His imidazole groups with the lipid head groups and other features of the membrane interface.

Notably, the helices with a single histidine at H16 or H14 [32] remain transmembrane under all conditions that have been observed, whereas the helices with H8 transition between transmembrane and surface states. Similarly, the helix with H12 is transmembrane at neutral pH yet transitions to the surface of DOPC bilayers at low pH [32]. Helices with H8 alone or with the (H8, H16) pair both transition, but differ in their dependence on the bilayer thickness. While GWALP23-H<sup>8,16</sup> shows multiple states in DMPC (Fig. 9; Table 3) at all pH values (Fig. 11), GWALP23-H<sup>8</sup> shows complex spectra (Fig. 4) that suggest multiple states in DOPC, and a pH-dependent transition in DMPC (Figs. 2, 5). Indeed, GWALP23-H<sup>8</sup> spans the DMPC bilayer at low pH but shows complex properties at high pH (Figs. 3, 5).

It is likely that two populations of the H8 helix are present in DOPC, as are seen for GWALP23-H<sup>8,16</sup> in DMPC. Also in thicker membranes of DEiPC lipid (C20:1; data not shown), GWALP23-H<sup>8</sup> continues to display multiple resonances, meaning the orientation transition is not yet complete and the peptide seems to struggle to move to a single orientation. With the presence of two histidines, the transition from transmembrane to surface orientation is perhaps easier for the GWALP23-H<sup>8,16</sup> helix. These results suggest furthermore that the multi-state behavior shown by GWALP23-H<sup>8,16</sup> is mostly influenced by H8, although the transition membrane identity changes when H16 is present as opposed to when H8 is alone in GWALP23-H<sup>8</sup>.

The dynamic extent of helix "wobble"  $\sigma_{\tau}$  about a mean tilt angle  $\tau_0$  differs between the transmembrane and surface orientations of the helices observed here. For a number of transmembrane helices, a low

value of about 5°-10° fits nicely for  $\sigma_{\tau}$  [44,59], regardless of whether the rotational "slippage"  $\sigma_{\rho}$  is moderate or very large [29,28]. But when the GWALP23-R<sup>8,16</sup> helix moves to the surface of DOPC bilayers [35],  $\sigma_{\tau}$  fits near 25° and not 5°. A similar observation holds for the corresponding double His helix, as  $\sigma_{\tau}$  fits near 35° and not near 10° when GWALP23-H<sup>8,16</sup> moves to a membrane surface (Table 3). These individual helices seem to experience greater flexibility of their helix tilt angle when on a membrane surface. Contrasting results were observed for some highly charged peptides such as (KIAGKIA)<sub>3</sub>, which exhibits low  $\sigma_{\tau}$  on a membrane surface but a higher value near 25° when inserted as a peptide assembly [48]. In either case, the  $\sigma_{\tau}$  fluctuations are fast on the NMR time scale because the resonances are sharp (e.g., Fig. 8).

pH Dependence In addition to lipid bilayer thickness, GWALP23-H<sup>8</sup> as well as GWALP23-H<sup>16</sup> is sensitive to pH, as the helices respond when the pH of the bilayer environment varies, notably even though the GWALP23-H<sup>8,16</sup> helix properties do not change with pH (Fig. 11). In DLPC and DMPC, titration points are observed for GWALP23-H<sup>8</sup> in the vicinity of pH 3.5 (Fig. 6). These low pKa values of a buried His residue show general agreement with those observed previously for GWALP23-H<sup>12</sup> and GWALP23-H<sup>14</sup> [32]. The results therefore suggest and confirm that the pKa of the His side chain decreases somewhat (as expected), to an extent that depends on the depth of burial of the imidazole ring, which also is observed for soluble proteins [60]. Among these mutants studied so far, the depth of burial of H12 is highest and that probably is the reason that H12 exhibits a pKa value below 3, the lowest pKa compared to the others.

Among the individual histidines, the results for titrating H16 are similar to changes observed for GWALP23-H<sup>14</sup> [32] or GWALP23-K<sup>14</sup> [30]. Each of these helices maintains a transmembrane orientation, with the side chain titration influencing the tilt and rotation of the helix. The extent of the rotational change is nevertheless much greater when titrating lysine than when titrating histidine. Interestingly, although H16 is located closer to the membrane interface compared to H14, the pKa of H16 is lowered (relative to the value in aqueous solution) to a somewhat greater extent. The proximity of H16 to the bulky indole ring of W19 may influence the pKa of H16.

A significant reduction in the <sup>2</sup>H NMR spectral quality (Fig. 5) suggests complex behavior and perhaps multiple states for the GWALP23-

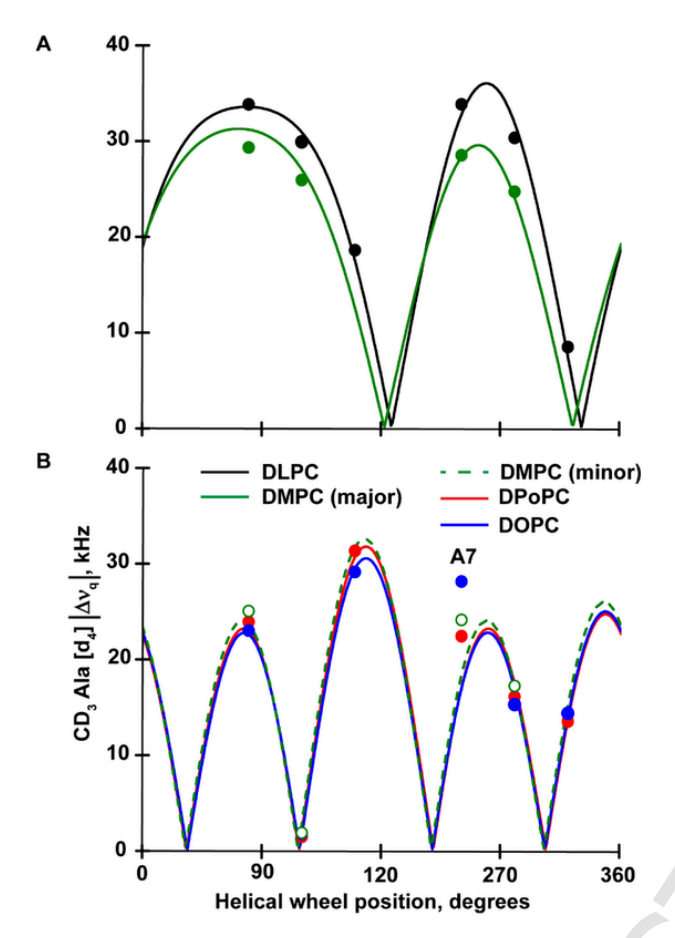


**Fig. 9.** Quadrupolar wave analysis depicting two different orientations of the GWALP23-H<sup>8,16</sup> helix with respect to DLPC, DMPC, DPoPC and DOPC bilayer membranes obtained by the GALA method [41]. Panel A shows the plots for transmembrane orientations with  $\tau_0 = 25^0$  in DLPC (solid black) and with  $\tau_0 = 22^0$  for the major population in DMPC (solid green). In panel B, each plot represents a surface orientation with tilt angle of  $\sim$ 87° for the minor population in DMPC (dashed green) and major populations in DPOPC (solid red) and DOPC (solid blue) lipids. Detailed results are listed in Table 3 and the orientation transitions are represented in Fig. 10. (For interpretation of the references to colour in this figure legend, the reader is referred to the web version of this article.)

H<sup>8</sup> helix at pH higher than 4 in DMPC bilayers. The complex properties persist in DOPC at all pH values (Fig. 4). By contrast, for GWALP23-H<sup>16</sup> in DOPC, the helix occupies a stable transmembrane state and the H16 side chain titrates with a pKa of about 3.5 (Fig. 6C), again typical for a submerged imidazole ring in a lipid bilayer. The influence of His titration upon the transmembrane helix orientation is in all cases modest, affecting the tilt of GWALP23-H<sup>8</sup> in DLPC by about only 3° and also the orientation of GWALP23-H<sup>16</sup> in DOPC by only 3° (Table 3). The small 3° change in each case reduces the helix tilt when the His imidazole ring is neutral (Table 3); a similar small change was observed when H14 of GWALP23-H<sup>14</sup> titrates [32]. The diverse properties of GWALP23-H<sup>8</sup> in DOPC and in DMPC at high pH reflect the sensitivity of the transmembrane helix to the precise location and ionization state of the His side chain. Notable GWALP23-H12 also occupies multiple states when the H12 ring is neutral yet proceeds to a major surface state at low pH [32].

The shift of pKa for a His imidazole ring in a membrane environment is indeed biologically relevant. For example, a pKa value of less than 2.3 was found for a buried histidine H149 in xylanase [60]. On the other hand, for H72 in bovine tyrosine phosphatase the pKa is close to 9 [61]. In the M2 ion channel of influenza A protein, the functionally important histidine residue H37 generates two different pKa values as the folded protein changes its conformation [62]. Another example involves the membrane insertion peptides such as pHLIP [63-65], which transitions from a membrane-inserted state to a surface orientation depending on the ionization of Asp residues [66,67]. Introduction of a His residue at the opposite face of the helix is predicted to yield a His pKa of about 4.7, which in turn can shift the pKa of Asp and thereby stabilize a membrane-inserted state within the 3.1-6.8 pH range [68]. Our results which reveal varying pKa values for histidine that also affect the multi-state properties, response to lipid thickness, and stability of a transmembrane state, are consistent with these studies of larger membrane protein systems.

## 5. Conclusions

In summary, we have employed the GWALP23 peptide framework to elucidate further the histidine side chain ionization properties and influence on helix properties when buried within the hydrophobic core of lipid bilayer membranes. Two buried  $\alpha$ -helical His residues essentially equidistant from the bilayer center each titrate individually with a low pKa between 3 and 4, but the pH dependence is no longer evident when both histidines are present. Notably, both transmembrane and surface orientations for the 23-residue helix are observed when H8 is present, with a membrane thickness dependence for the transition between the two states. The thickness dependence is modulated by the presence of H16, but the surface orientation is not observed with H16 alone. The findings support a minor extent of snorkeling for histidine side chains, in line with previous observations for arginine and lysine. The results, including the observed prominent effect of H8 over H16 for the properties of the GWALP23-H<sup>8,16</sup> helix, highlight the importance and complexity of individual and pairwise histidine interactions for regulating the properties of membrane proteins.

# Transparency document

The Transparency document associated with this article can be found, in online version.

# Declaration of competing interest

The authors declare no conflict of interest.

## Acknowledgments

This work was supported in part by grant MCB 1713242 from the United States National Science Foundation, and by the Arkansas Biosciences Institute.

## Appendix A. Supplementary data

Supplementary data to this article can be found online at https://doi.org/10.1016/j.bbamem.2020.183501.

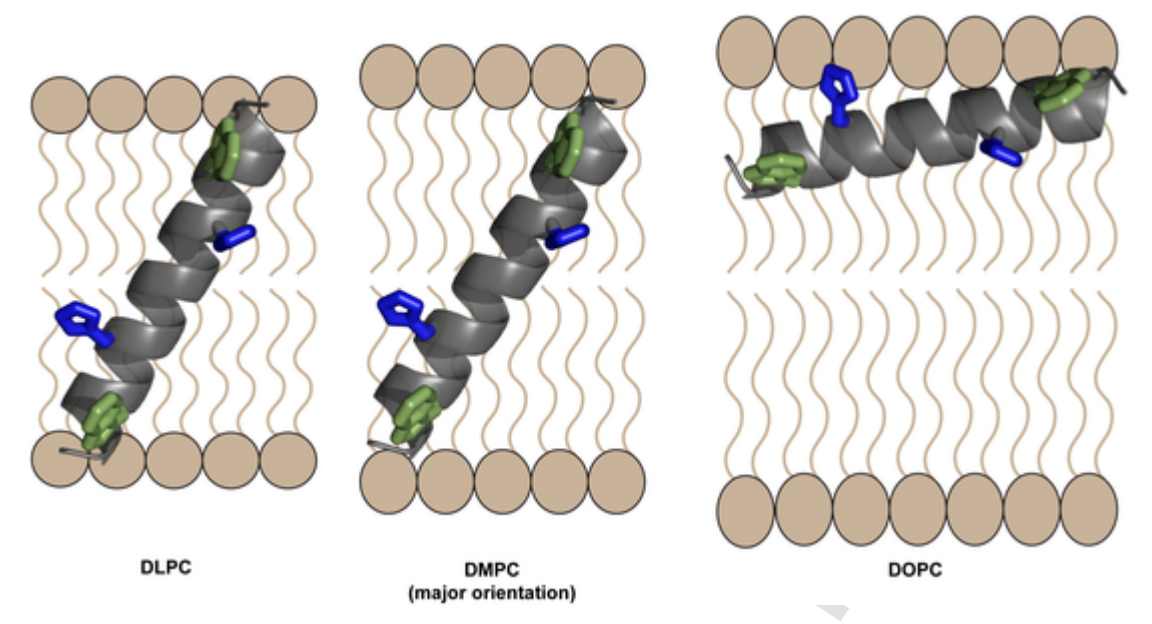


Fig. 10. Models to illustrate the transition of GWALP23-H<sup>8,16</sup> from its tilted transmembrane orientation (in DLPC) to a primary orientation at the surface of DOPC bilayer membranes. In the bilayer of intermediate thickness, DMPC, the major population of the helix adopts a transmembrane orientation with slightly smaller tilt than in DLPC, shown in the center panel. The minor population in DMPC has a surface bound orientation (not shown) similar to that in DOPC (right panel).

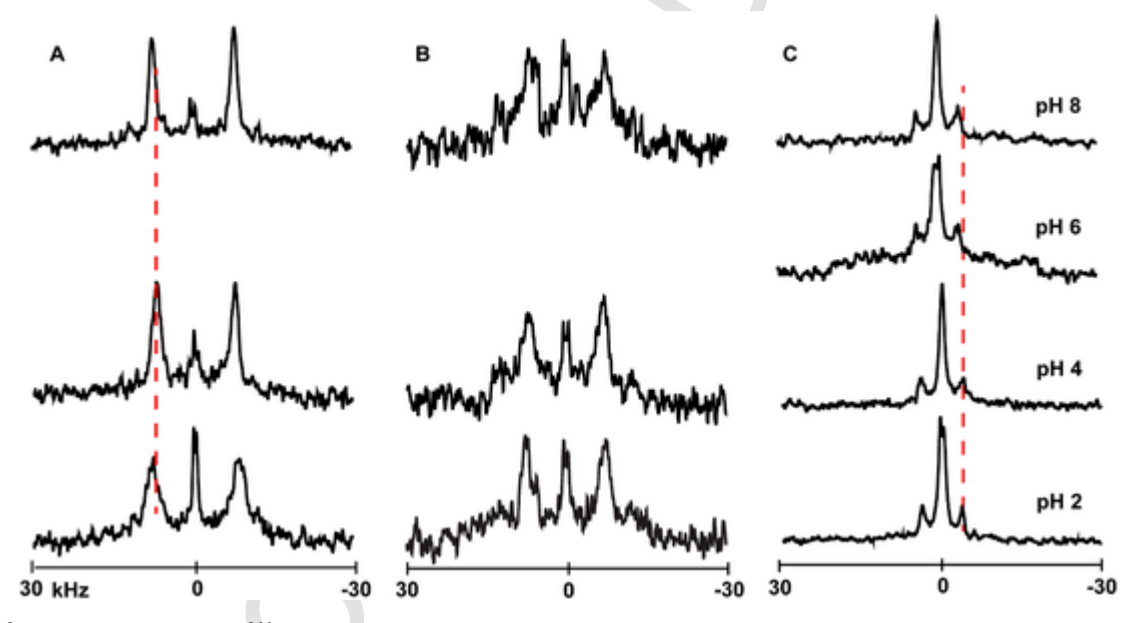


Fig. 11. Selected  $^2H$  NMR spectra of GWALP23-H $^{8,16}$  labeled alanines A11 and A13 in the core helix in DLPC (A), DMPC (B) and DOPC (C) lipid bilayers hydrated with 20 mM buffer at the indicated pH. Sample orientation is  $\beta=90^\circ, 1:60$  peptide:lipid at 50  $^\circ$ C.

## References

- [1] M. Rehwald, F. Neuschafer-Rube, C. de Vries, G.P. Puschel, Possible role for ligand binding of histidine 81 in the second transmembrane domain of the rat prostaglandin f-2 alpha receptor, FEBS Lett. 443 (1999) 357–362.
- [2] A.K. Stewart, C.E. Kurschat, D. Burns, N. Banger, R.D. Vaughan-Jones, S.L. Alper, Transmembrane domain histidines contribute to regulation of ae2-mediated anion exchange by pH, Am. J. Physiol. Cell Physiol. 292 (2007) C909–C918.
- [3] C.A. Larson, P.L. Adams, B.G. Blair, R. Safaei, S.B. Howell, The role of the methionines and histidines in the transmembrane domain of mammalian copper transporter 1 in the cellular accumulation of cisplatin, Mol. Pharmacol. 78 (2010) 232, 230
- [4] R. Loewenthal, J. Sancho, A.R. Fersht, Histidine aromatic interactions in barnase elevation of histidine pKa and contribution to protein stability, J. Mol. Biol. 224 (1992) 759–770.

- [5] E. Cauet, M. Rooman, R. Wintjens, J. Lievin, C. Biot, Histidine-aromatic interactions in proteins and protein-ligand complexes: quantum chemical study of x-ray and model structures, J. Chem. Theor. Comp. 1 (2005) 472–483.
- [6] A. Jasanoff, M.A. Weiss, Aromatic histidine interactions in the zinc finger motifstructural inequivalence of phenylalanine and tyrosine in the hydrophobic core, Biochemistry 32 (1993) 1423–1432.
- [7] J. Fernández-Recio, A. Vázquez, C. Civera, P. Sevilla, J. Sancho, The tryptophan/histidine interaction in  $\alpha$ -helices, J. Mol. Biol. 267 (1997) 184–197.
- [8] R. Bhattacharyya, R.P. Saha, U. Samanta, P. Chakrabarti, Geometry of interaction of the histidine ring with other planar and basic residues, J. Proteome Res. 2 (2003) 255–263.
- [9] F.H. Hu, K. Schmidt-Rohr, M. Hong, NMR detection of pH-dependent histidine-water proton exchange reveals the conduction mechanism of a transmembrane proton channel, J. Am. Chem. Soc. 134 (2012) 3703–3713.
- [10] P. Venkataraman, R.A. Lamb, L.H. Pinto, Chemical rescue of histidine selectivity filter mutants of the M2 ion channel of influenza a virus, J. Biol. Chem. 280 (2005) 21463–21472.
- [11] A. Perier, A. Chassaing, S. Raffestin, S. Pichard, M. Masella, A. Menez, V. Forge, A. Chenal, D. Gillet, Concerted protonation of key histidines triggers membrane

- interaction of the diphtheria toxin T domain, J. Biol. Chem. 282 (2007) 24239\_24245
- [12] A.S. Ladokhin, pH-triggered conformational switching along the membrane insertion pathway of the diphtheria toxin t-domain, Toxins 5 (2013) 1362–1380.
- [13] I.V. Kurnikov, A. Kyrychenko, J.C. Flores-Canales, M.V. Rodnin, N. Simakov, M. Vargas-Uribe, Y.O. Posokhov, M. Kurnikova, A.S. Ladokhin, pH-triggered conformational switching of the diphtheria toxin t-domain: the roles of n-terminal histidines, J. Mol. Biol. 425 (2013) 2752–2764.
- [14] S.B. Prusiner, Prions, Proc. Natl. Acad. Sci. U. S. A. 95 (1998) 13363-13383.
- [15] A. Malevanets, et al., Interplay of buried histidine protonation and protein stability in prion misfolding, Sci. Rep. 7 (2017) 882.
- [16] B. Bechinger, Towards membrane protein design: pH-sensitive topology of histidine-containing polypeptides, J. Mol. Biol. 263 (1996) 768–775.
- [17] C. Aisenbrey, E. Goormaghtigh, J.M. Ruysschaert, B. Bechinger, Translocation of amino acyl residues from the membrane interface to the hydrophobic core: thermodynamic model and experimental analysis using ATR-FTIR spectroscopy, Mol. Membr. Biol. 23 (2006) 363–374.
- [18] C. Aisenbrey, R. Kinder, E. Goormaghtigh, J.M. Ruysschaert, B. Bechinger, Interactions involved in the realignment of membrane-associated helices - an investigation using oriented solid-state NMR and attenuated total reflection Fourier transform infrared spectroscopies, J. Biol. Chem. 281 (2006) 7708–7716.
- [19] B. Perrone, A.J. Miles, E.S. Salnikov, B.A. Wallace, B. Bechinger, Lipid interactions of LAH4, a peptide with antimicrobial and nucleic acid transfection activities, Eur. Biophys. J. Biophys. Lett. 43 (2014) 499–507.
- [20] B. Vogt, P. Ducarme, S. Schinzel, R. Brasseur, B. Bechinger, The topology of lysine-containing amphipathic peptides in bilayers by circular dichroism, solid-state NMR, and molecular modeling, Biophys. J. 79 (2000) 2644–2656.
- [21] V.V. Vostrikov, B.A. Hall, D.V. Greathouse, R.E. Koeppe 2nd, M.S. Sansom, Changes in transmembrane helix alignment by arginine residues revealed by solid-state NMR experiments and coarse-grained md simulations, J. Am. Chem. Soc. 132 (2010) 5803–5811.
- [22] V.V. Vostrikov, B.A. Hall, M.S. Sansom, R.E. Koeppe 2nd, Accommodation of a central arginine in a transmembrane peptide by changing the placement of anchor residues, J. Phys. Chem. B 116 (2012) 12980–12990.
- [23] M.J. McKay, R. Fu, D.V. Greathouse, R.E. Koeppe II, Breaking the backbone: central arginine residues induce membrane exit and helix distortions within a dynamic membrane peptide, J. Phys. Chem. B 123 (2019) 8034–8047.
- [24] B. Bechinger, D.A. Skladnev, A. Ogrel, X. Li, E.V. Rogozhkina, T.V. Ovchinnikova, J.D.J. O'Neil, J. Raap, N-15 and P-31 solid-state NMR investigations on the orientation of zervamicin II and alamethicin in phosphatidylcholine membranes, Biochemistry 40 (2001) 9428–9437.
- [25] E.S. Salnikov, B. Bechinger, Lipid-controlled peptide topology and interactions in bilayers: structural insights into the synergistic enhancement of the antimicrobial activities of PGLa and magainin 2, Biophys. J. 100 (2011) 1473–1480.
- [26] U.S. Sudheendra, B. Bechinger, Topological equilibria of ion channel peptides in oriented lipid bilayers revealed by N-15 solid-state NMR spectroscopy, Biochemistry 44 (2005) 12120–12127.
- [27] N.J. Gleason, V.V. Vostrikov, D.V. Greathouse, C.V. Grant, S.J. Opella, R.E. Koeppe 2nd, Tyrosine replacing tryptophan as an anchor in GWALP peptides, Biochemistry 51 (2012) 2044–2053.
- [28] S.L. Grage, E. Strandberg, P. Wadhwani, S. Esteban-Martin, J. Salgado, A.S. Ulrich, Comparative analysis of the orientation of transmembrane peptides using solid-state H-2- and N-15-NMR: mobility matters, Eur. Biophys. J. Biophys. Lett. 41 (2012) 475–482.
- [29] V.V. Vostrikov, C.V. Grant, S.J. Opella, R.E. Koeppe 2nd, On the combined analysis of <sup>2</sup>H and <sup>15</sup>N/<sup>1</sup>H solid-state NMR data for determination of transmembrane peptide orientation and dynamics, Biophys. J. 101 (2011) 2939–2947.
- [30] N.J. Gleason, V.V. Vostrikov, D.V. Greathouse, R.E. Koeppe 2nd, Buried lysine, but not arginine, titrates and alters transmembrane helix tilt, Proc. Natl. Acad. Sci. U. S. A. 110 (2013) 1692–1695.
- [31] J.K. Thibado, A.N. Martfeld, D.V. Greathouse, R.E. Koeppe, Influence of high pH and cholesterol on single arginine-containing transmembrane peptide helices, Biochemistry 55 (2016) 6337–6343.
- [32] A.N. Martfeld, D.V. Greathouse, R.E. Koeppe 2nd, Ionization properties of histidine residues in the lipid bilayer membrane environment, J. Biol. Chem. 291 (2016) 19146–19156.
- [33] V. Rajagopalan, D.V. Greathouse, R.E. Koeppe 2nd, Influence of glutamic acid residues and pH on the properties of transmembrane helices, BBA - Biomembranes 1859 (2017) 484–492.
- [34] F. Afrose, R.E. Koeppe, Comparing interfacial Trp, interfacial His and pH dependence for the anchoring of tilted transmembrane helical peptides, Biomolecules 10 (2020) 273.
- [35] K. Lipinski, M.J. McKay, F. Afrose, A.N. Martfeld, R.E. Koeppe 2nd, D.V. Greathouse, Influence of lipid saturation, hydrophobic length and cholesterol on double-arginine-containing helical peptides in bilayer membranes, ChemBioChem 20 (2019) 2784–2792.
- [36] P.B.W. Kortenaar, B.G. Dijk, J.M. Peeters, B.J. Raagen, P.J. Adams, G.I. Tesser, Rapid and efficient method for the preparation of Fmoc-amino acids starting from 9-fluorenylmethanol, Int. J. Pept. Prot. Res. 27 (1986) 398–400.
- [37] D.V. Greathouse, R.E. Koeppe II, L.L. Providence, S. Shobana, O.S. Andersen, Design and characterization of gramicidin channels, Methods Enzymol. 294 (1999) 525–550.

- [38] C. Aisenbrey, B. Bechinger, Investigations of polypeptide rotational diffusion in aligned membranes by 2H and 15N solid-state NMR spectroscopy, J. Am. Chem. Soc. 126 (2004) 16676–16683.
- [39] E. Salnikov, C. Aisenbrey, V. Vidovic, B. Bechinger, Solid-state NMR approaches to measure topological equilibria and dynamics of membrane polypeptides, BBA-Biomembranes 1798 (2010) 258–265.
- [40] C.N. Pace, F. Vajdos, L. Fee, G. Grimsley, T. Gray, How to measure and predict the molar absorption coefficient of a protein, Protein Sci. 4 (1995) 2411–2423.
- [41] P.C. van der Wel, E. Strandberg, J.A. Killian, R.E. Koeppe 2nd, Geometry and intrinsic tilt of a tryptophan-anchored transmembrane alpha-helix determined by <sup>2</sup>H NMR, Biophys. J. 83 (2002) 1479–1488.
- [42] J.H. Davis, K.R. Jeffrey, M.I. Valic, M. Bloom, T.P. Higgs, Quadrupolar echo deuteron magnetic resonance spectroscopy in ordered hydrocarbon chains, Chem. Phys. Lett. (1976) 390–394.
- [43] E. Strandberg, S. Esteban-Martin, A.S. Ulrich, J. Salgado, Hydrophobic mismatch of mobile transmembrane helices: merging theory and experiments, Biochim. Biophys. Acta 1818 (2012) 1242–1249.
- (44) K.A. Sparks, N.J. Gleason, R. Gist, R. Langston, D.V. Greathouse, R.E. Koeppe 2nd, Comparisons of interfacial Phe, Tyr, and Trp residues as determinants of orientation and dynamics for GWALP transmembrane peptides, Biochemistry 53 (2014) 3637–3645.
- [45] J.M. Resende, C.M. Moraes, V.H.O. Munhoz, C. Aisenbrey, R.M. Verly, P. Bertani, A. Cesar, D. Pilo-Veloso, B. Bechinger, Membrane structure and conformational changes of the antibiotic heterodimeric peptide distinctin by solid-state NMR spectroscopy, Proc. Natl. Acad. Sci. U. S. A. 106 (2009) 16639–16644.
- [46] J.M. Resende, R.M. Verly, C. Aisenbrey, A. Cesar, P. Bertani, D. Pilo-Veloso, B. Bechinger, Membrane interactions of phylloseptin-1, -2, and -3 peptides by oriented solid-state NMR spectroscopy, Biophys. J. 107 (2014) 901–911.
- [47] E. Strandberg, A. Grau-Campistany, P. Wadhwani, J. Burck, F. Rabanal, A.S. Ulrich, Helix fraying and lipid-dependent structure of a short amphipathic membrane-bound peptide revealed by solid-state NMR, J. Phys. Chem. B 122 (2018) 6236–6250.
- [48] E. Strandberg, D. Bentz, P. Wadhwani, A.S. Ulrich, Chiral supramolecular architecture of stable transmembrane pores formed by an alpha-helical antibiotic peptide in the presence of lysolipids, Sci. Rep. 10 (2020) 4710.
- [49] C. Aisenbrey, B. Bechinger, Tilt and rotational pitch angle of membrane-inserted polypeptides from combined N-15 and H-2 solid-state NMR spectroscopy, Biochemistry 43 (2004) 10502–10512.
- [50] B. Bechinger, J.M. Resende, C. Aisenbrey, The structural and topological analysis of membrane-associated polypeptides by oriented solid-state NMR spectroscopy: established concepts and novel developments, Biophys. Chem. 153 (2011) 115–125.
- [51] J. Pan, S. Tristram-Nagle, N. Kucerka, J.F. Nagle, Temperature dependence of structure, bending rigidity, and bilayer interactions of dioleoylphosphatidylcholine bilayers, Biophys. J. 94 (2008) 117–124.
- [52] N. Kucerka, M.P. Nieh, J. Katsaras, Fluid phase lipid areas and bilayer thicknesses of commonly used phosphatidylcholines as a function of temperature, Biochim. Biophys. Acta 1808 (2011) 2761–2771.
- [53] A.N. (Martfeld) Henderson, Influence of Histidine Residues, pH and Charge Interactions on Membrane-Spanning Peptides Ph. D. Dissertation University of Arkansas, 2017 (108 pages).
- [54] E. Strandberg, S. Morein, D.T.S. Rijkers, R.M.J. Liskamp, P.C.A. van der Wel, J.A. Killian, Lipid dependence of membrane anchoring properties and snorkeling behavior of aromatic and charged residues in transmembrane peptides, Biochemistry 41 (2002) 7190–7198.
- [55] K. Ojemalm, T. Higuchi, P. Lara, E. Lindahl, H. Suga, G. von Heijne, Energetics of side-chain snorkeling in transmembrane helices probed by nonproteinogenic amino acids, Proc. Natl. Acad. Sci. U. S. A. 113 (2016) 10559–10564.
- [56] E. Strandberg, J.A. Killian, Snorkeling of lysine side chains in transmembrane helices: how easy can it get?, FEBS Lett. 544 (2003) 69–73.
- [57] S.S. Krishnakumar, E. London, The control of transmembrane helix transverse position in membranes by hydrophilic residues, J. Mol. Biol. 374 (2007) 1251–1269.
- [58] B. Bechinger, Solid-state NMR investigations of interaction contributions that determine the alignment of helical polypeptides in biological membranes, FEBS Lett. 504 (2001) 161–165.
- [59] F. Afrose, M.J. McKay, A. Mortazavi, V. Suresh Kumar, D.V. Greathouse, R.E. Koeppe 2nd, Transmembrane helix integrity versus fraying to expose hydrogen bonds at a membrane-water interface, Biochemistry 58 (2019) 633–645.
- [60] L.A. Plesniak, G.P. Connelly, W.W. Wakarchuk, L.P. McIntosh, Characterization of a buried neutral histidine residue in *Bacillus circulans* xylanase: NMR assignments, pH titration, and hydrogen exchange, Protein Sci. 5 (1996) 2319–2328.
- 61] P.A. Tishmack, D. Bashford, E. Harms, R.L. Van Etten, Use of <sup>1</sup>H NMR spectroscopy and computer simulations to analyze histidine pK(a) changes in a protein tyrosine phosphatase: experimental and theoretical determination of electrostatic properties in a small protein, Biochemistry 36 (1997) 11984–11994.
- [62] M.T. Colvin, L.B. Andreas, J.J. Chou, R.G. Griffin, Proton association constants of His 37 in the influenza-A M2(18-60) dimer-of-dimers, Biochemistry 53 (2014) 5987–5994.
- [63] J.F. Hunt, P. Rath, K.J. Rothschild, D.M. Engelman, Spontaneous, pH-dependent membrane insertion of a transbilayer alpha-helix, Biochemistry 36 (1997) 15177–15192.
- [64] O.A. Andreev, A.G. Karabadzhak, D. Weerakkody, G.O. Andreev, D.M. Engelman, Y.K. Reshetnyak, pH (low) insertion peptide (pHLIP) inserts across a lipid bilayer

- as a helix and exits by a different path, Proc. Natl. Acad. Sci. U. S. A. 107 (2010) 4081-4086
- [65] F.N. Barrera, J. Fendos, D.M. Engelman, Membrane physical properties influence transmembrane helix formation, Proc. Natl. Acad. Sci. U. S. A. 109 (2012) 14422–14427.
- [66] J. Westerfield, C. Gupta, H.L. Scott, Y.J. Ye, A. Cameron, B. Mertz, F.N. Barrera, Ions modulate key interactions between pHLIP and lipid membranes, Biophys. J. 117 (2019) 920–929.
- [67] M. Bano-Polo, L. Martinez-Gil, F.N. Barrera, I. Mingarro, Insertion of bacteriorhodopsin helix c variants into biological membranes, ACS Omega 5 (2020) 556–560.
- [68] D. Vila-Vicosa, T.F.D. Silva, G. Slaybaugh, Y.K. Reshetnyak, O.A. Andreev, M. Machuqueiro, Membrane-induced pK(a) shifts in wt-pHLIP and its l16h variant, J. Chem. Theor. Comp. 14 (2018) 3289–3297.
- [69] W.L. DeLano, The PyMOL molecular graphics system, The PyMOL Molecular Graphics System, Delano Scientific, San Carlos, CA, 2002.
- [70] V.V. Vostrikov, A.E. Daily, D.V. Greathouse, R.E. Koeppe 2nd, Charged or aromatic anchor residue dependence of transmembrane peptide tilt, J. Biol. Chem. 285 (2010) 31723–31730.
- [71] V.V. Vostrikov, C.V. Grant, A.E. Daily, S.J. Opella, R.E. Koeppe 2nd, Comparison of "polarization inversion with spin exchange at magic angle" and "geometric analysis of labeled alanines" methods for transmembrane helix alignment, J. Am. Chem. Soc. 130 (2008) 12584–12585.